Design and Development of an Affordable Haptic Robot with Force-Feedback and Compliant Actuation to Improve Therapy for Patients with Severe Hemiparesis

Andrew Theriault, Mark Nagurka, and Michelle J. Johnson, *Member, IEEE*

Abstract—The study describes the design and development of a single degree-of-freedom haptic robot, Haptic Theradrive, for post-stroke arm rehabilitation for in-home and clinical use. The robot overcomes many of the weaknesses of its predecessor, the TheraDrive system that used a Logitech steering wheel as the haptic interface for rehabilitation. Although the original TheraDrive system showed success in a pilot study, its wheel was not able to withstand the rigors of use. A new haptic robot was developed that functions as a drop-in replacement for the Logitech wheel. The new robot can apply larger forces in interacting with the patient, thereby extending the functionality of the system to accommodate low-functioning patients. A new software suite offers appreciably more options for tailored and tuned rehabilitation therapies. In addition to describing the design of the hardware and software system, the paper presents the results of simulation and experimental case studies examining the system's performance and usability.

Index Terms—Haptic Applications, Haptics Technology, Force-Feedback, Rehabilitation

1 Introduction

ROBOTS have a long-term role to play in the rehabilitation of stroke survivors [1], [2], [3]. One possible role is as a therapy assistant in areas away from hospitals and inpatient rehabilitation centers. By developing more affordable robotic-haptic-mechatronic systems, nursing homes and adult daycare centers can benefit from the use of robot therapy systems. For this reason, there is a trend towards creating less expensive systems that can achieve functional treatment outcomes. Past examples of low-cost therapy systems highlight lessons learned that inform the development of effective low-cost solutions for neurorehabilitation.

1.1 Lessons Learned from Low Cost, Therapy Systems

Lesson 1: Game therapy with low-cost systems can reduce motor impairment. Palanca was an early mechatronic system that automated the rehabilitation process using a game [4]; it consists of a slider on a 1 m track, interfaced with a computer for use as a game controller. Four subjects used Palanca to play Pong, 30 minutes per day, five days per week, for a total of 13 sessions; overall subjects showed significant functional improvements of the impaired arm.

Lesson 2: Low-cost force-feedback robotic systems can be effective and elicit increased impaired arm use, especially in training higher functioning subjects with more strength. Driver's SEAT, developed by Johnson et al. [5], introduced a low-cost driving simulator interface for rehabilitation robots. It uses a force-feedback split-steering wheel with a force sensor for each hand that enabled the robot to respond differently to force inputs from each hand. In this case, the robot resists forces applied by a stroke patient's unimpaired arm, forcing the patient to use the impaired arm to assist in the completion of steering tasks. Eight stroke subjects tested the system. Low functioning had the most difficulty learning from the force cues and tended to fight the wheel especially in wheel positions that required them to rotate against gravity.

Lesson 3: Commercial force-feedback systems can be used as meaningful assessment tools; performance metrics derived from their use are sensitive to motor function level. JavaTherapy ,the TheraJoy system and UniTherapy software were developed to investigate the use of commercial force feedback gaming joysticks as therapy robots in an under-supervised environment [6], [7], [8]. In [7], Joysticks were used to perform positioning and tracking exercises with the UniTherapy software, a web-based interface that allows both the therapist and the patient to design and execute tracking exercises [8]. Force feedback was used to provide assistive or resistive forces to the patient during the execution of movements. Sixteen high-

- *A. Theriault is with the Department of Mechanical Engineering, Marquette University, Milwaukee, WI, 53233. E-mail: andrew.theriault @marquette.edu.*
- *M. Nagurka is with the Department of Mechanical Engineering, Marquette University, Milwaukee, WI, 53233. E-mail: mark.nagurka @marquette.edu.*
- *M. J. Johnson was with the Department of Biomedical Engineering, Marquette University, WI, 53233 and the Department of Physical Medicine and Rehabilitation, Medical College of Wisconsin, Milwaukee, WI, 53226. She is now with the Department of Physical Medicine and Rehabilitation, University of Pennsylvania, 1800 Lombard Street, Philadelphia, PA 19146. E-mail:johnmic@mail.med.upenn.edu.*

Digital Object Indentifier 10.1109/ToH.2013.51 1939-1412/13/$31.00 © 2013 IEEE

and low-functioning stroke subjects and eight unimpaired subjects performed exercise with TheraJoy/UniTherapy. Subject performance on exercises with UniTherapy was calculated using root-mean-square tracking error, percentage of time on target, and mean time to target [8]. The system distinguished between functional levels.

Lesson 4: Low-cost therapy systems suffer from several drawbacks. One challenge is posing interesting tasks in training stroke survivors. Another challenge is faced in training very low functioning subjects with severe hemiparesis. The inability to create adequate force-feedback to assist the impaired limb and the inability to adapt to the non-uniform strength needs across the task space limit the effectiveness for low-functioning stroke survivors.

The next section details challenges encountered in the early use of TheraDrive, a low-cost computer-aided robotic system for stroke therapy. The above lessons including those learned from using Theradrive lead to design requirements for a low-cost, Haptic version of Theradrive.

1.2 Lessons Learned from Low Cost, Force-Feedback and Game Therapy with TheraDrive

TheraDrive builds on the successes of Driver's SEAT and TheraJoy, using off-the-shelf force feedback steering wheels (Logitech Wingman) as therapy robots with a single degree-of-freedom [7], [8], [9]. The steering wheel is mounted on a tilting frame (0-90 degrees) and then to a height adjustable frame (0.45m – 0.81m). By moving the robot from front to side and adjusting the angle of the wheel forces, the upper limb is used in different planes of motion. A crank handle, which the patient grips, is mounted to the wheel. Fig. 1 shows the Theradrive set-up where a subject is shown seated in the side drive mode.

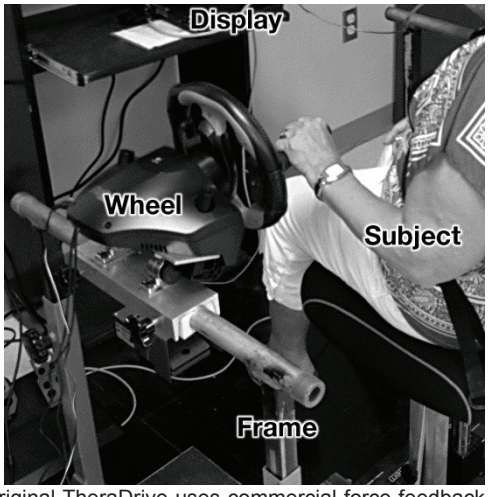

Fig.1. Original TheraDrive uses commercial force-feedback steering wheel from Logitech™.

Rote or Fun therapy with TheraDrive is designed to increase the range of motion (ROM) of the elbow in flexion/extension and the shoulder in flexion/extension and internal/external rotation. For rote therapy, the patient is presented with a point-to-point positioning task or a trajectory-following task by the UniTherapy software program. The wheel is used to move a cursor to a specified point or to guide the cursor along a moving path. The therapist can select from a large array of point layouts and trajectory shapes to adjust the task difficulty to the ability of the patient. Fun (or Game) therapy involves having the patient play a computer game using the wheel as a controller.

Assistive or resistive forces can be generated and the magnitude of these forces is set by the therapist before each exercise. This assistance/resistance usually takes the form of a virtual spring that attracts/repels the patient from the target position, but it can be changed to emulate a mass, a damper, or random perturbations.

The TheraDrive system was evaluated with 10 subjects, who underwent 24 one-hour training sessions over six to eight weeks [9]. Subjects were divided into two groups: rote therapy only and game therapy only. Subjects were evaluated using metrics including the Fugl-Meyer scale and the Ashworth test for spasticity. Both groups showed improvements in motor function and decreases in spasticity, but the sample size was too small to determine statistical significance. The game-based therapies enhanced the motivation and engagement of patients and resulted in a slight increase in functionality gain over simple tracking and positioning exercises. However, several limitations were observed.

Some subjects needed more assistance to complete tasks than the system could provide. One stroke survivor in the pilot study was unable to use his hand for grasping and had very little arm movement. He relied on a support sling for his forearm and upper arm to perform the exercises. This underscored the need to improve the wheel interface to provide better support for low-functioning stroke survivors who have difficulty with hand opening/closing and difficulty supporting the forearm against gravity.

The game controllers used in the TheraDrive system do not perform as desired. The maximum force-feedback moment produced by the wheel is not sufficient and can be overcome by some patients. The small brushed DC motor driving the wheel is underpowered, supplying 1.5 N-m of torque at the end-effector [5]. This means that the wheel cannot be used to build strength in all patients or to emulate a rigid constraint. Another difficulty with the wheel is its inability to withstand off-axis forces and moments. Uncoordinated patients often exert lifting or bending forces on the wheel.

The wheel uses plastic-on-plastic bushings (not roller bearings), shortening its already short wear life even further due to increased loading on its surfaces. The sliding surfaces produce a significant amount of wear debris, which embeds itself between the teeth, causing damage to the molded plastic gears. The gears have considerable backlash and compliance, both of which increase with wear. The backlash creates a dead zone where the force feedback does not influence the wheel's motion. Several Logitech wheels wore out over the course of the pilot study as a result of the large forces exerted in the normal

and tangential directions.

Patient-specific adaptive control is an important feature that the TheraDrive system lacks. Patients experience differing levels of impairment at different points in their range of motion, and ideally the controller would account for this to deliver personalized therapy. The current controller is only able to simulate a constant stiffness linear spring. This means that during an exercise, patients can move the wheel with great difficulty at some points along its travel and with relative ease at other points. A controller that adapts to each patient's impairment, based upon range of motion, torque, and speed is needed.

1.3 Requirements for the Haptic TheraDrive

To circumvent the limitations of the TheraDrive system, a new Theradrive robot, called Haptic Theradrive (Fig. 2), has been developed. The new system functions as a more powerful "drop-in replacement" for the Logitech wheel that can safely exert larger forces on the patient during therapy. It thus extends its functionality to accommodate low-functioning patients. Key design requirements include:

1. The "drop-in replacement" is a computer-controlled force-feedback robot that must fit into the existing Theradrive system and be able to mount to the adjustable frame in front and on the sides, allowing exercises to be performed in different planes.
2. The robot must be low-cost to maintain the affordable theme (less than $3000 USD).
3. The robot must support torques on the crank larger than 25 N-m (220 in-lb). This value was determined from preliminary work with Driver's SEAT [5] where it was found that low functioning subjects could, with trunk involvement, overpower a tangential resistance force of 50 N.
4. The controller must be patient-specific and adapt to forces at the crank to accommodate a variety of stroke patients, especially low-functioning patients with motor weakness and poor coordination.
5. The robot must be backdrivable and operate safely (that is, be torque limited).
6. The forces on the crank arm of the robot must be measurable.

Requirements 3-6 represent key advancements over the original Theradrive system. Due to stronger actuation, higher force assistance/resistance forces can be applied and done so safely using a new compliant torque limiter. A new crank handle measures tangential and normal forces (using a custom force sensor) during steering and allows for a wider range of motion. Adaptive control algorithms afford more responsive to the level of impairment and motor performance.

The Haptic Theradrive system (Fig. 2) trains subjects in similar ways as the earlier Theradrive. The therapy goal is to improve range of motion and strength in the elbow and shoulder by having subjects practice tracking tasks with the robot in different configurations resulting from adjusting the height of the frame, angle of the robot, and the level and strategy of force-feedback.

1.4 Achieving High-Forces and Compliance

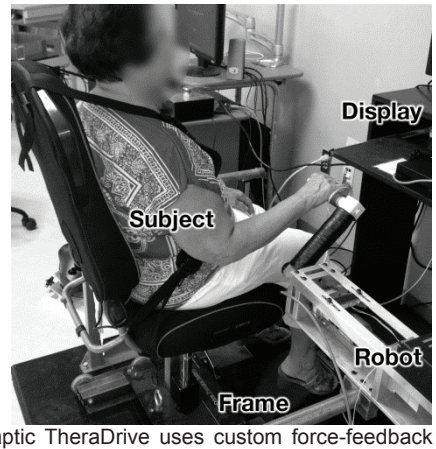

Fig. 2. Haptic TheraDrive uses custom force-feedback crank and fits into the TheraDrive frame to allow use of the crank in front drive or side drive configurations.

Other haptic robot systems have been proposed for the stroke therapy which are able to generate higher forces during training to support more impaired stroke survivors [10], [11], [12] . However, the issue of ensuring that the human-subject interaction is compliant and safe despite high forces is a matter for research.

Achieving high forces and safe human-robot interactions with impaired subjects is not trivial. Collisions between a stiff robot and a human can cause injury to the human and potentially damage the robot. To ensure safe human-machine interaction, robot actuators must have some amount of compliance. Compliant actuation is a sharp departure from that used in industrial robotics, where robots and actuators are made with near infinite stiffness. Van Ham et al. describe several strategies of producing a compliant actuator [14]. The simplest suggested method is a series elastic actuator (SEA), consisting of a stiff actuator in series with a compliant element such as a spring. The performance of this actuator is limited because the stiffness cannot be adapted to different operating conditions without increasing the complexity of the control law. With variable stiffness, the compliant element of a SEA is no longer passive as the actuator stiffness is partially governed by the controller.

Variable-stiffness (VS) actuators overcome this limitation by introducing a second degree-of-freedom that controls the stiffness of the joint. One method uses mechanically-controlled stiffness, where the actuator stiffness is adjusted by moving the compliant element. The VS joint developed by the DLR in Germany is an example [15]. It consists of rollers pressed against a cam by a set of springs. The position and stiffness of the joint are controlled independently by a drive motor and a smaller motor that adjusts the preload in the spring. When the joint is deflected, the rollers are pushed up by the cam, compressing the spring. The spring restoring force pushes the rollers back towards the equilibrium position. Changing

the shape of the cam allows for different spring types to be emulated, with progressive, degressive, or linear stiffness.

In order for the new haptic Theradrive robot to apply large forces to the patient safely, a torque limiter is added to the robot's transmission. The transmission is also made to be compliant to protect the patient from impact loads during a sudden reversal of the motor or during an accidental collision between patient and robot. Both of these requirements are met using a single transmission element, a compliant torque limiter that is essentially a cross between a drill clutch and the VS Joint. Due to this transmission element in concert with the motor, gear, sensors, and custom force sensor etc., the new Haptic TheraDrive can support a low functioning subject.

1.5 Achieving Force-Feedback & Adaptive Control

Force-feedback is used to define a training environment that is appropriate for subjects at different functioning levels. Since safety is of utmost concern, developing a stable controller is highest priority. The goal is to minimize the risk of human injury from large unexpected robot movements. The design of the system must balance transparency and stability to achieve a stable system with a small effective inertia.

Closed-loop control of a force feedback system can be implemented using an impedance or admittance approach. The strategy of coupling force-feedback with adaptive control is frequently used in rehabilitation robotics to permit robots to kinematically and dynamically adjust to function level and motor performance. For example, one is an assist-as-needed approach [16] where the robot gives as little assistance as possible to get the patient as close to a desired trajectory as possible. This approach can be viewed as an optimization problem with an objective function,

$$J = \frac{\lambda_1}{2} e^2 + \frac{\lambda_2}{2} F^2, \quad (1)$$

that is minimized, reflecting a weighted sum of patient error e and assistive force F. Solving this optimization problem yields the desired assist-as-needed control law. However, solving this problem requires a priori knowledge of the relationship between assistance and error. For this reason, this strategy may work best with model-based controllers. This minimization strategy was used by Reiner et al. in an assisted gait study. By adaptively scaling the reference leg trajectory, a new commanded leg trajectory was created that fit within each subject's walking speed and range of motion and had the same shape as a healthy gait trajectory [17].

Adaptive control can also be used to alter the difficulty of an exercise based on subject performance. Several strategies exist from tuning the tracking task variability to tuning the field strength based on the subject's spatial or temporal performance error. For example, the Wrist-Robot developed by Masia and colleagues implemented this adaptive strategy to tune the difficulty level alongside a nonadaptive assist-as-needed controller [12]. With this robot subjects tracked oscillating trajectories in the three rotational degrees-of-freedom of the wrist. The assistive controller created a virtual quadratic spring that attracted the subjects to the desired wrist orientation. After each period of oscillation, the adaptive controller incremented the oscillation frequency while simultaneously decrementing the frequency by an amount proportional to the mean absolute tracking error over the previous period of oscillation.

A slightly different strategy was adopted by Columbo et al. [18]. Here the level of assistance during reaching tasks was modified based on a priori training task performance and decisions of the therapist based on difficulty levels during the training. An adaptive strategy emulated the decision-making process of a trained physical therapist, allowing the robot to select tasks with a subject specific level of assistance.

Vergaro et al. and Casadio et al. [19], [20] directly modified the assistive field for a planar robot based on tracking error and movement time. The tracking exercises consist of following a continuous path divided into segments. An assistive force field is rendered to attract subjects to the path, but it does not impose any constraint on velocity along the path. The subject's tracking error and movement duration for completed segments along the path are measured. If both of these performance metrics are less than pre-defined thresholds, the magnitude of the assistive force field is decremented. This implements "assist-as needed" control by gradually eliminating assistance that is not necessary.

In our study, we focus on developing an adaptive strategy that improves upon the a priori tuning of spring resistance or assistance employed in TheraDrive. The original TheraDrive used impedance control (in which force is a function of position and its derivatives). Impedance control is also used in the new Haptic Theradrive in conjunction with an adaptive control strategy to enable the the controller to respond to the subject's functional level and control effort during tracking.

The following sections describe the following [21]: 1) the mechanical, electrical, and software design of the new Haptic Theradrive system meeting the above requirements, and 2) simulation and actual experiments with two human subjects (1 able-bodied and 1 low-functioning) to evaluate the feasibility of the system. The potential benefits of this new design for home therapy are also discussed.

2 Haptic TheraDrive Design Features

2.1 Achieving Increased Forces with a Low-cost Mechanical and Electrical Design

An actuator that can output mechanical power of the same order of magnitude as the human arm would fulfill the first specific aim and provide patients with large supportive forces. Due to budget and weight constraints, the motor selected was an aftermarket treadmill motor (Turdan Industry C9J06J). It is a 2-pole brushed DC motor rated at 2175 W (2.9 HP) at 70% duty cycle with a maximum speed of 8000 rpm and with windings rated for 130 V. Motor constants are back emf constant, k_e = 0.155 V/rad/s, and torque constant, k_T = 0.155 N-m/A. Although the motor is rated for rotation in one direction only, its windings and commutator are symmetrical, so it achieves the same performance in both directions. The motor is overpowered for this application, but through the servo amplifier's voltage/current limiters and a custom mechanical torque limiter, the maximum mechanical power delivered to the patient is 950W (1.27 HP, that is, 400 in-lb at 200 rpm). A maximum output torque of 45 N-m (400 in-lb) translates to a linear force at the end effector of 222 N (50 lb), a value on the same order of magnitude as the linear output force of the human arm at the hand.

Coupling the motor to the end effector is a planetary gearbox (Anaheim Automation GBPH0602-NP040) with a 40:1 gear reduction ratio. This reduces the maximum end effector linear velocity to 4.3 m/s (14 ft/s), about triple the speed of a normal reaching movement. A planetary gearbox was selected over a harmonic drive because the planetary gearbox is more easily backdriven, allowing for smoother haptic interaction. A flexible spider coupling was added between the motor's output shaft and the gearbox to reduce shock loads on the gearbox and lengthen the expected life of the gears.

Driving the motor is a plug-in analog PWM servo amplifier (Advanced Motion Control, model 30A 20AC) interfaced with a DAQ system. Built-in voltage and current limiters allow the amplifier to limit the maximum velocity and torque of the motor. A 1000-line hollow-shaft rotary optical encoder (Red Lion, model ZPJ1000A) was mounted directly to the output shaft of the robot. With x4 decoding (four counts per quadrature cycle), the resolution of measured end effector position is 32 counts per cm (80 counts per in.). The index of the encoder is aligned with the center of the robot workspace, where the crank arm is vertical, corresponding to the starting position of every exercise trajectory. Encoder signals are filtered digitally by the encoder DAQ board (Measurement Computing, QUAD-04).

The motor and gearbox are mounted to an aluminum chassis. The chassis mounts to the same frame as the original TheraDrive using two clamps. The robot in the therapy environment is pictured in Fig. 2. Like the original TheraDrive, the Haptic TheraDrive robot can be reconfigured on the TheraDrive mounting frame. By adjusting the height of the frame and the position of the robot, the system can be fitted to each patient. The workspace of the robot is a 270-degree circular arc, with a radius of 200 mm (8 in), corresponding to the path of the crank. Mechanical stops prevent the crank from making multiple revolutions

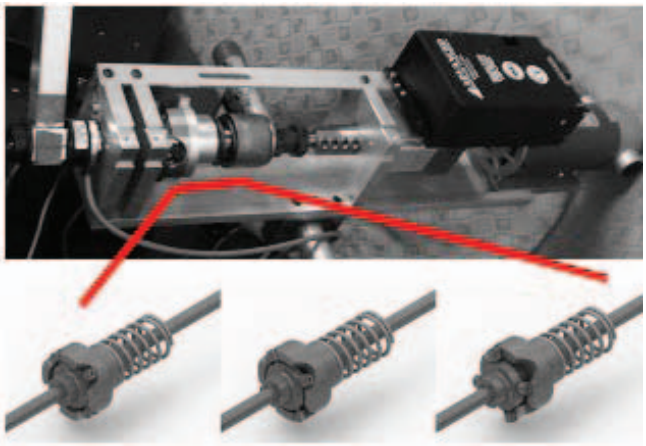

Fig. 3. A close up of the robot internal components showing a custom compliant torque limiter (top). The compliant torque limiter is shown in three stages in the CAD drawing: Equilibrium, Transmitting torque and Over-torque (from left to right). The line indicates where the component appears.

to avoid damage to the wiring. Compared to the Logitech wheel, the haptic robot has double the workspace radius and 50% more angular travel. Motions targeted by therapy with the system are elbow flexion/extension, shoulder flexion/extension, and internal/external shoulder rotation.

2.2 Custom Compliant Torque Limiter

The custom mechanical compliant torque limiter consists of a crown cam, splined to the input shaft, and a cam follower keyed to the output shaft, see Fig. 3. The cam is held against the follower by a spring, but it is free to slide along the spline of the input shaft. Thrust bearings are placed on both sides of the limiter to take thrust loads off of the bearings in the gearbox and output shaft. Deflecting the output shaft causes the cam to compress the spring, generating a restoring torque. This creates a torsional spring from a linear spring, and the stiffness profile of the torsional spring can be altered by changing the shape of the cam surface. In an overload condition, the cam leaves the followers, disengaging the output shaft.

For an angular deflection of θ, the restoring torque T(θ) is defined by the relationship

$$T(\theta) = \frac{dz}{d\theta} r_c \left(F_{ko} + kz(\theta)\right) \quad (2)$$

where z(θ) defines the shape of the cam surface, r_c is the cam radius, k is the linear spring stiffness, and F_{ko} is the preload in the spring. The preload in the spring is adjusted manually using a telescoping shaft collar to compress the spring. The torque limits are determined in part by the depth and slope of the cam profile and can be adjusted by varying the preload in the spring. The cam shape chosen for this robot is parabolic. With a parabolic cam path, increasing the preload in the spring increases the torsional stiffness. When the spring preload is low, this provides patients who cannot handle large interaction forces a softer robot to reduce discomfort.When the spring preload is high, the robot is able to exert larger forces at the end effector without excessive output shaft

deflection. The equation for restoring torque with a parabolic cam path of $z(\theta) = a\theta^2$ becomes

$$T(\theta) = 2a\theta r_c F_{ko} + 2ka^2 r_c \theta^3. \quad (3)$$

The cam motion is assumed to be quasi-static, as the spring force is much greater than the inertia of the moving parts. This assumption holds true except when the cam leaves the overloaded condition, moving from the flat surface to the steep parabolic surface. This is acceptable because exercises with the robot are aborted if the torque limiter is overloaded (Fig 3b).

To size the cam to a chosen spring, five parameters must be known: the minimum torque limit, T_{min}; the maximum torque limit, T_{max}; the spring stiffness, k; the spring force at maximum compression, F_{max}; and the desired cam radius, r_c. The cam profile is parabolic, defined as of $z(\theta) = a\theta^2$, and the profile depth is z_{max}.

The maximum angular deflection before the follower leaves the cam then becomes

$$\theta_{max} = \sqrt{z_{max}/a} \quad (4)$$

and the cam slope at this point is

$$\frac{dz}{d\theta_{max}} = 2\sqrt{az_{max}}. \quad (5)$$

The minimum torque limit is realized when there is zero preload in the spring, giving the equation

$$T_{min} = \left(2\sqrt{az_{max}}\right)(r_c)(kz_{max}) \quad (6)$$

The maximum torque limit is realized when the spring is at full compression when the follower leaves the cam, giving the equation

$$T_{max} = \left(2\sqrt{az_{max}}\right)(r_c)(F_{max} - kz_{max}). \quad (7)$$

This creates a system of two equations which can be solved for a and z_{max} to determine the cam shape. A final check must be done to verify that the determined cam shape will fit the allotted space without overlapping itself or creating thin features that would fail under load. If this check is failed, a different spring must be chosen.

The spring for the torque limiter has a stiffness of 144 N/cm (82 lb/in) and a load of 609 N (137 lb) at full compression. Minimum and maximum torque limits were chosen as T_{min} = 9 N-m (80 in-lb) and T_{max} = 45 N-m (400 in-lb), respectively, and the cam radius was chosen to be 3.8 cm (1.5 in). With a crank arm radius of 20 cm (8 in), these torque limits correspond to 44 and 222 N (10 and 50 lb) of tangential force at the end effector, respectively. Solving the above equations yields a cam profile of $z(\theta) = 14.8\theta^2$ cm ($5.81\theta^2$ in) with a depth of z_{max} = 10.6 mm (0.418 in). Since the center of the cam follower must trace this profile, the physical cam surface is offset normal to the cam profile by the radius of the follower, 6.4 mm (0.25 in) in this case. The cam profile is repeated four times around the cam circumference in order to quadruple the mechanical strength of the torque limiter by using four cam followers and to balance the distribution of the spring force.

TABLE 1: CAM DESIGN PARAMETERS

Parameter	IPS Value	SI Value
k	82 lb/in	144 N/cm
F_{max}	137 lb	609 N
r_c	1.5 in	3.8 cm
T_{min}	80 in-lb	9 N-m
T_{max}	400 in-lb	45 N-m
a	5.81 in/rad/rad	14.8 cm/rad/rad
z_{max}	0.418 in	1.06 cm

The minimum and maximum torque limits were tested by hanging barbells from the end effector with the crank arm below the horizontal position. The motor shaft was turned manually until either the crank arm rose past the horizontal position or the torque limiter disengaged. If the torque limiter did not disengage, the torque limit was not exceeded. With the torque limiter set to its minimum limit, the crank was able to lift a weight of 44 N (10 lb) but not a weight of 66 N (15 lb). With the torque limiter at its maximum limit, the crank was able to support a weight of 200 N (45 lb) but not a weight of 222 N (50 lb).

This showed good agreement with the theoretical values of 10lb (44N) at the minimum limit and 50lb (222N) at the maximum limit. Table 1 summarizes the Cam parameters.

2.3 Custom Force Sensor in Crank Handle

To measure the human-robot interaction forces, a load cell was built into the crank handle. These interaction forces are needed to close the impedance control loop and for data collection during experiments/exercises. The compliant element of the drivetrain could not be used to measure torque because its stiffness is variable and nonlinear, and thus a load cell is used. The load cell is composed of a cantilever beam with eight strain gauges (Vishay Micro-Measurements, 062LW) mounted to the crank arm. The beam has a circular cross-section and a conical taper, narrowing towards the free end, to maximize strain in areas under low load. This, in turn, increases the sensitivity of the load cell by maximizing the strain experienced by each strain gauge. The handle grip is fitted around the load cell and rotates freely on bearings. Fixing the load cell to the arm rather than the grip allows forces to be measured in the radial-tangential coordinate system of the crank arm and simplifies the conversion of interaction forces to joint-space torque. Strain gauges are mounted around the circumference of the beam at 90-degree intervals at two points along its length, as shown by the alignment marks drawn in Fig. 4a. Diametrically opposed gauges are wired in a half-bridge configuration and measure bending strains at two points due to moments about the radial and tangential axes, for a total of four measured strains. The half-bridge configuration provides temperature compensation.

a.

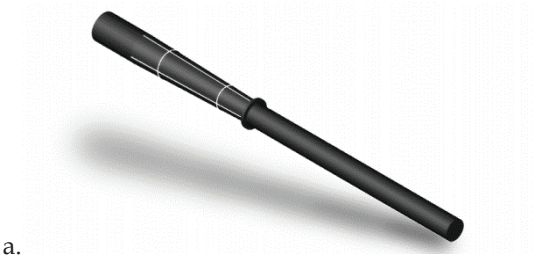

b.

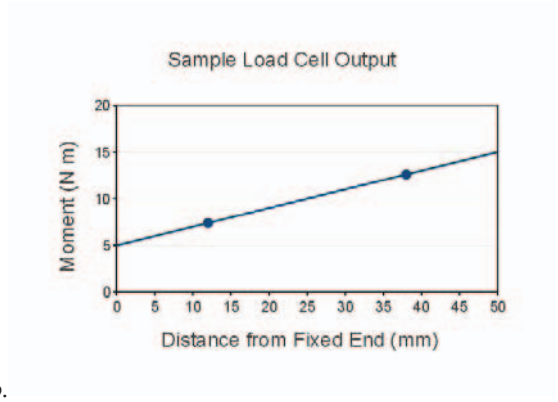

Fig. 4a. Custom crank handle with strain gauge mounting at the cross line and 4b. Illustration of how shear and moment reactions at the end of the beam are related to the moments measured at the gauges.

The strain gauge bridge amplifier is designed around the Burr-Brown INA125 instrumentation amplifier with precision voltage reference, a chip designed to power strain gauges and amplify strain gauge signals. Four strain gauge half-bridges in the load cell produce four voltage signals proportional to strain along specific axes at specific points.

The four strains are used to calculate bending stresses, bending moments, and shear and moment reactions at the fixed end of the beam. The interaction force is converted to joint-space torque by multiplying the tangential shear reaction force by the crank arm radius, and this is used as the feedback to the impedance controller. The other three reactions are used only for clinical data collection. Calculation of the shear and moment reactions at the fixed end of the beam can be illustrated with a moment diagram (bending moment plotted as a function of position along the beam, as in Fig. 4b. Measured strains at the tangential gauge bridges are converted to bending moments using Hooke's Law and bending stress equations. A straight line is drawn through these two points, and the slope of the line is equal to the shear reaction, and the value of the line at the fixed end is the moment reaction. This procedure is repeated for the radial gauges.

The load cell was calibrated by clamping the fixed end to a workbench and hanging weights (8.9N to 53.4N) from points along the length of the beam (25 to 200 mm from end) and then recording the voltage outputs of the strain gauge bridge amplifier. From the value of the weight and its distance from the fixed end of the beam, the shear and moment reactions could be calculated. Least-squares planar regressions were performed to find the shear and moment reactions, each as a function of the two amplifier outputs after offset nulling. The correlation squared was greater than 0.99, indicating a very good fit of the plane to the data. The reactions for the tangential direction are

$$V = 94.26E_p - 292.7E_d\ N \tag{8}$$

$$M = 0.802E_p - 10.91E_d\ N \cdot m, \tag{9}$$

where V and M are the shear and moment reactions, respectively, and E_p and E_d are the voltage outputs of the amplifier from the bridges proximal and distal to the fixed end of the beam. Force and moment data for loads exceeding 12 lb (53.4N) must be extrapolated from this data. This was deemed acceptable because strain gauges are highly linear force sensors when mounted to linear elastic materials, and the beam was designed not to undergo plastic deformation until 445 N (100 lb) was applied to the tip.

2.4 Software Design

2.4.1 Control Design

The Haptic Theradrive robot is controlled using a dedicated computer running Mathworks Simulink xPC Target OS for real-time control and data acquisition. This PC is fitted with two DAQ boards to read sensors and communicate with the servo amp: an encoder board from Measurement Computing (PCI-QUAD04) and a multipurpose board from National Instruments (NI PCI-6251). A host computer running Matlab interfaces with the target computer through an ethernet connection to upload executable binaries and display the patient interface.

Control of the robot is achieved through three loops, all running at a sample rate of 1000 Hz to allow for smooth controller response. The control architecture is illustrated in Fig. 5. The innermost control loop is the impedance proportional-integral-derivative (PID) controller. This controller was designed and tuned in simulation using Matlab's Control System Toolbox. The topology of the impedance controller is PID with feedforward, taking a force command and force feedback at the input and producing a motor current signal at the output. The feedforward path consists of a constant multiplied by the signum of the end effector velocity in order to cancel the effects of Coulomb friction. After tuning in simulation, the PID controller gains found were used as a starting point for manual tuning of the impedance controller on the real robot. The PID controller gains used, in current output per force error, are k_p=0.0760 A/N, k_i=0.645 A/N-s, and k_d=0.000897 A-s/N. The feedforward term is 0.616 A. Stability of the controller was analyzed using root loci. The z-domain poles of this controller lie within the unit circle, so the controller is stable, and the impedance loop as a whole is stable because the mechanical plant (mass-spring-mass) is inherently also stable.

The intermediate loop is the assistive/resistive controller, which renders a force field in the robot's workspace.

The controller divides the workspace into 17 regions, spaced 1/16th of a revolution apart. Each region has a value assigned to it to define the assistive/resistive stiffness of the robot at that location, with negative stiffnesses being assistive and positive stiffnesses being resistive. It is necessary to implement position-dependent stiffness be-

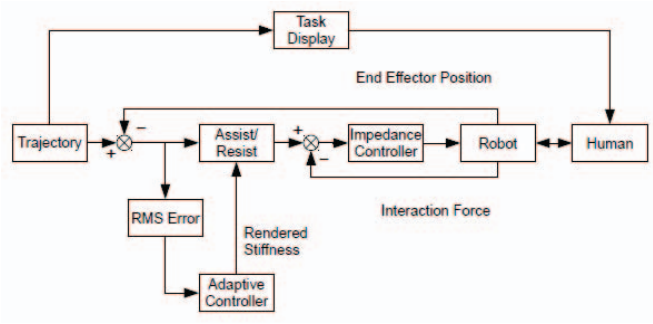

Fig. 5. Control Flow Chart

cause stroke patients usually have inconsistent abilities in the range of motion of their impaired arm. The stiffnesses between regions are interpolated to produce smooth transitions between regions of different stiffnesses. Assistive stiffness is rendered as a linear spring pulling the patient towards the target end effector position with a small damper added to reduce overshoot. Resistive stiffness is rendered as a linear spring that repels the patient from the target position, creating an unstable system that the patient must stabilize. For patients requiring assistance, the stiffnesses are either zero or negative so the patient only receives assistance. The opposite is true for patients requiring resistance.

The outermost control loop is the adaptive controller. It uses a strategy similar to that [12] and [18] but runs continuously instead of in discrete steps. The controller evaluates patient performance in real-time and continuously adapts the stiffness of the robot to the patient's ability. Since patient performance depends in part upon the amount of assistive/resistive stiffness, altering the stiffness will cause a change in patient performance. Patient performance is quantified as the root-mean-square (RMS) trajectory tracking error over the past three seconds, a metric chosen because it was used to quantify subject performance in the original TheraDrive. This error is compared to a desired error of 0.25 rad (2 in or 51 mm of arc length), a value corresponding to the width of the target that the patient tracks. A nonzero tracking error is desired because this maintains difficulty of exercises. If the desired tracking error were zero, the robot would always provide maximum assistance to every patient, and if the desired tracking error were too large, the robot would maximum resistance to patients. Stiffness values in a quadrant centered around the end effector are adjusted proportionally to the difference between actual and desired tracking error, essentially establishing a proportional control loop around the gains of the assistive/resistive controller. Over time, the adaptive controller shapes the stiffness profile to suit the patient's ability level, ensuring that exercises will be difficult but doable and that the patient will not be assisted more than is necessary. ``Difficult but doable'' means that patients should be presented with a challenge sufficient to maintain motivation and a moderate degree of exertion, but the challenge should not be so great as to cause patients to become frustrated or to fail to complete exercises.

For testing purposes, the adaptive controller has several operating modes that disable some or all of its features, allowing for specific variables to be isolated in experiments. Zero impedance mode disables all assistance and resistance and makes the end effector behave as if it were rotating freely. Static assist/resist modes disable the adaptive controller and provide a fixed stiffness. These first two modes emulate the behavior of the original TheraDrive system with the wheel rotating freely or with spring assist/resist, respectively, allowing for a direct comparison of the two systems in testing. Plain adaptive mode provides adaptive stiffness but disables position-dependent stiffness. Position-dependent adaptive mode enables all features of the adaptive controller. Table 2 summarizes the mode.

TABLE 2: CONTROL FEATURES

Mode	Assist/Resist	Adaptive	Crank Position Dependent
Zero-impedance	No	No	No
Constant Spring	Yes	No	No
Adaptive Spring	Yes	Yes	No
Position Adaptive	Yes	Yes	Yes

2.4.2 Task Software

The task software on the host computer is made to emulate the appearance of UniTherapy to the patient, allowing it to satisfy the first specific aim of creating a drop-in replacement. The interface presents the patient with an arrow cursor that follows the position of the end effector, seen in Fig. 6. The cursor is situated at the bottom of the screen, and the desired trajectory scrolls down the screen towards the cursor, presenting a blue box at the current target location. The cursor changes from red to green while it is within the target box. The framerate of this task display is approximately 33 Hz, the same as that of UniTherapy.

The operator interface uses Matlab scripts to automate random trajectory generation and data uploading to the robot. Most functions can be performed with a single command at the Matlab command line. Data is automatically streamed via Universal Datagram Protocol (UDP) from the robot to the host computer during exercises and saved to the Matlab workspace. The streamed data packets contain a timestamp, commanded and actual position, commanded and actual haptic interaction force, off-axis forces, and controller gains. After an exercise is complete, the data can be saved to a file for later analysis.

Fig. 6. GUI of Tracking Task

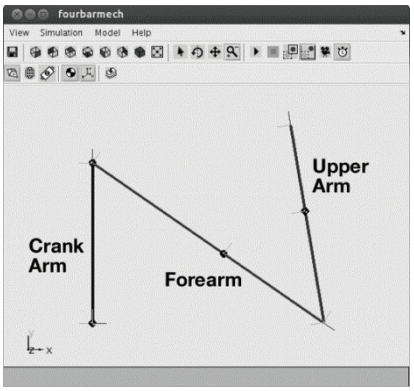

Fig.7. Simulated Model is a graphical representation of the simulation model. The crank arm is on the left and the human forearm and upper arm is on the right. For the moderate subject in (13): a=0.25 and b=1

3 Simulation and Human Subject Cases

A simulation model was created based upon the characteristics of the real system, and care was taken to ensure the model had good fidelity to the real hardware. It models all of the major mechanical components of the robot as well as the robot controllers described in Table 2. A simulated human arm from another project was added to model the interaction between human and robot. This model was used for the initial tuning of the impedance PID controller and for the first experiments with the adaptive controller, discussed in the following.

3.1 Simulation Design

A model of the robot and human patient was written in Mathworks Matlab, Simulink, and SimMechanics to aid in controller design and testing without risk of injury. The crank and human arm were modeled as a four-bar linkage, with the motor coupled to the crank through a nonlinear spring. Parameters for the model robot, such as link inertia and motor torque constant, were found through characterization of the motor and through analysis of 3D part drawings in SolidWorks. Equations of motion were created and solved numerically within SimMechanics based upon the mechanical model. Using SimMechanics, all nonlinearities in the system, such as encoder quantization and Coulomb friction, could be modeled easily, and a more accurate model of the system than a linearized analytic model was produced. The human arm model was ported from another computational model created by Formica et al. for use with the MIT-Manus robot [22].

This model simulates the dynamics and control of the human arm with or without stroke impairment. It is a planar model consisting of a forearm/wrist segment, an elbow joint, an upper arm segment, and a fixed shoulder joint. The forearm/wrist segment is 35cm long with a mass of 1.54 kg, and the upper arm is 25cm long with a mass of 1.96kg, corresponding to metrics of a human of average height and weight. The simulation model is shown graphically in Fig. 7. A trajectory planner and joint-space proportional-derivative (PD) controller are used to model human control of the arm.

The PD controller is of the form

$$\begin{Bmatrix} T_e \\ T_s \end{Bmatrix} = \begin{bmatrix} P_{ee} & P_{se} \\ P_{es} & P_{ss} \end{bmatrix} \begin{Bmatrix} u_e \\ u_s \end{Bmatrix} + \begin{bmatrix} D_{ee} & D_{se} \\ D_{es} & D_{ss} \end{bmatrix} \begin{Bmatrix} \dot{u}_e \\ \dot{u}_s \end{Bmatrix}. \quad (11)$$

where u is the position error vector in rad in joint space and T is the joint torque output vector in N-m. The PD controller gains are based on the stiffness and viscoelasticity of the average human arm. The resulting controller gains have cross-coupling terms that reflect mono- and bi-articular muscle control. The gains in (12) are P_{ee}=8.67 Nm/rad, P_{se} =2.83 Nm/rad, D_{ee} = 0.76 Nm/rad/s, D_{se} = 0.18 Nm/rad/s, P_{es}=2.51 Nm/rad, P_{ss} =10.8 Nm/rad, D_{es} = 0.18 Nm/rad/s and D_{ss} = 0.63 Nm/rad/s.

The MIT-Manus arm model also contains a trajectory planner that simulates human trajectory planning in point-to-point movements, but this part of the model was not used because exercises consist of trajectory tracking rather than point-to-point movements, and trajectories are already defined in trajectory tracking tasks. Stroke impairment is simulated in the Manus model by perturbing the desired arm trajectory with a triangle function, creating a new trajectory that deviates from the ideal trajectory to simulate the disjointed piecewise trajectories taken by a stroke-impaired arm. For example, if the ideal trajectory were defined as $\theta(t)$, the perturbed trajectory, $\theta_p(t)$, would be defined as

$$\theta p(t) = \theta(t) + a\left(\theta(t) mod\ b - \frac{b}{2}\right), \quad (12)$$

where a and b define the amplitude and period of deviation, setting the severity of the simulated impairment. The mod operator gives the remainder of the devision. The arm then attempts to follow this perturbed trajectory, while the robot tries to follow the unperturbed trajectory. The trajectories used in exercises are a sum of four sine waves of different frequency and phase that create a pseudorandom smooth path.

3.2 Experiment Design and Hypothesis

To verify that the adaptive controller was able to adapt properly to patients with varying levels of impairment, simulations of the system were run with the MIT-

MANUS human arm model [22]. The first simulation was run with the unimpaired arm model to verify that the adaptive controller was stable, i.e., the resistive stiffness would settle to a steady-state. An exercise was run for ten minutes of simulation time, in position-dependent adaptive mode starting with assistive/resistive gains of zero, and the controller was allowed to adapt to the arm's performance. The average assistive/resistive gain as a function of time was recorded for the duration of the simulation. This procedure was then repeated for a simulated stroke patient to verify that the adaptive controller would be stable when adapting to a stroke-impaired subject. It was expected that the controller gain would show a first-order decay towards a steady-state value, with the controller providing resistance to the unimpaired and assistance to the impaired arm model. A first-order response from the adaptive controller was expected because it is a simple proportional controller with a first-order transfer function.

To verify that the position-dependent aspect of the adaptive controller functioned properly, the stroke arm model was used [22]. The perturbation function used to simulate impairment was set such that the maximum perturbation would occur at ±1 rad, where an angular position of 0~rad corresponds to the crank pointing straight up. A simulated exercise was run for ten minutes of simulation time, starting with an assistive/resistive gain of zero, and the controller was allowed to adapt to the arm's performance. Assistive/resistive gain as a function of end effector position was recorded after the simulation was completed. The plot of gain versus position was expected to show peaks in assistive gain at ±1 rad, where the tracking error of the arm was highest.

To compare simulation results to real tracking, two subjects were asked to use the system. One able-bodied subject without neurological injury and another stroke subject with a low to moderate function as defined by a upper limb Fugl-meyer score of 29 [23]. Subjects were seated at the Haptic TheraDrive and were asked to track a sinusoid in the zero-impedance mode and the position dependent adaptive mode (Table 2). The sinusiod was a sum of four sinusoids, centered about the vertical crank position, of amplitude 0.5 rad and frequencies of 0.5, 1.0, 1.5 and 2.0 rad/s (Fig. 6). The relative phases of the sinusoids were randomized for each exercise to reduce learning effects. RMS error was used as the comparison metric to examine accuracy compared to the simulation study.

4 Results

4.1 Simulated Healthy Versus Stroke Subjects

The baseline performance of the healthy and stroke patient models in a sine tracking exercise is displayed in Fig. 8a. Both models tracked the trajectory with the robot controller running in zero-impedance mode. The healthy model tracks the trajectory with little error, but the stroke model has large errors at the points where the spatial perturbation is at a maximum.

Figure 8b shows the adaptive controller responding to the performance of a simulated healthy patient. A sine tracking exercise was run for ten minutes of simulation time, and the resistive stiffness, averaged over the workspace, was plotted versus time. The controller response is approximately first-order with a time constant of 90 seconds, showing oscillations at steady state. Steady-state oscillations have the same period of oscillation as the sinusoidal trajectory.This was confirmed by cross correlation analysis.

The performance of a simulated healthy patient before and after controller adaptation is shown in Figure 8c. The baseline performance of the patient with zero resistance had RMS tracking error well below the target level of 0.25 rad, so the adaptive controller added resistance to the exercise until the target error was achieved. With the resistive gain adapted, the patient was still able to track the reference trajectory, but with an increase in error from 0.058 rad at baseline to 0.230 rad with resistance. This increase in tracking error is apparent in Figure 8c.

The response of the adaptive controller to a simulated stroke patient is shown in Figure 8d. The assistive gain is plotted over time during a ten-minute sine tracking exer-

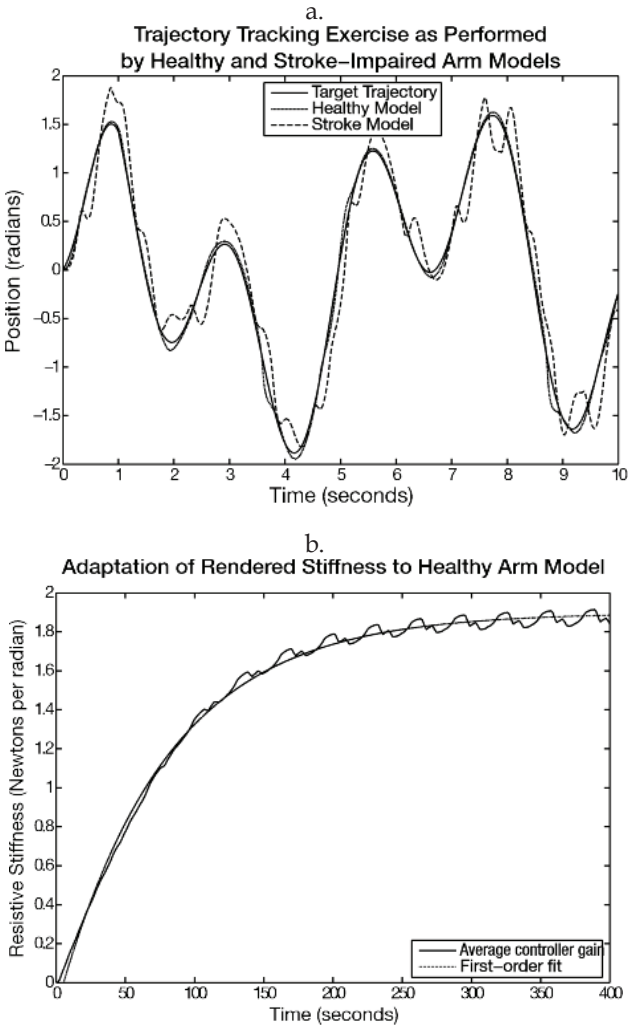

Fig.8a. Simulated Tracking Task with Healthy Model and Stroke Model and 8b. Rendered Stiffness being adapted to healthy subject performance.

cise. The controller response shows first-order decay with a 90 second time constant and oscillations at steady state with the same period as the tracked trajectory (12.6 seconds). RMS tracking error decreases from 0.307 rad over the first 30 seconds to 0.265 rad over the last 30 seconds.

Figures 8b and 8d show the adaptive controller modifying the stiffness of the robot to suit the ability levels of a simulated healthy subject and simulated stroke subject. With zero resistance, the healthy subject tracks the trajectory very closely, but after the adaptive controller adds resistance, the RMS tracking error increases to the desired level of 0.25 rad. The tracking error of the stroke subject decreased until it reached the desired level as the controller gains were adapted. This demonstrates the ability of the adaptive controller in simulation to adjust the stiffness of the robot to achieve a desired level of performance from a subject.

Oscillations in controller gains, plotted in Figures 8b and 8d, are caused by the shape of the trajectories the patients are tracking. This is because there are slight variations of difficulty in the motions that compose the trajectory. For example, tracking fast movements is more difficult than tracking slow movements, so changes in the trajectory velocity will perturb the gains of the adaptive controller.

Performance of the position-dependent adaptive controller with a simulated stroke subject is displayed in Figure 9. The triangle perturbation function used to simulate impairment was defined to have peaks at ±1 rad, causing maximum perturbation of the trajectory at the aforementioned peaks. A sine tracking exercise was run until the adaptive controller reached steady state, and the resulting gains were plotted. This graph shows two peaks where the assistive gain is larger (more negative): one large peak at 1rad and a smaller, wider peak at -1.3 rad. These peaks correspond roughly to the locations where perturbation of the trajectory to simulate stroke was largest (±1 rad).

Position-dependent assistive gain is important for therapy exercises with stroke patients, as they have varying levels of ability throughout the robot's workspace. Figure 8e shows the assistive gain of the simulated robot plotted against end effector position. The peaks in the gain correspond roughly with the locations of peak trajectory perturbation in the stroke subject model. The peaks are of different magnitudes due to the differing mechanical advantage of the arm at these points. At -1.3 rad, the arm is extended and has little mechanical advantage over the robot, and less assistance is required to correct tracking errors. However, at 1 rad, the arm is close to the body, giving the patient a large mechanical advantage, so more assistance is required to correct the trajectory.

Mechanical advantage is also the reason the peak at -1.3 rad was shifted from the expected position of -1 rad. The mechanical advantage of the patient is lower at the angle of -1 rad than at -1.3 rad because around -1 rad, there is a point where the tangent to the path of the elbow intersects with the axis of the crank, creating a singularity in the kinematics. At this point, the shoulder joint has zero mechanical advantage over the crank because it cannot exert any moment on it, putting the arm's overall mechanical advantage at a minimum. The arm has more mechanical advantage at -1.3 rad, so more assistance is required at this point to correct the arm's trajectory than is required at -1 rad.

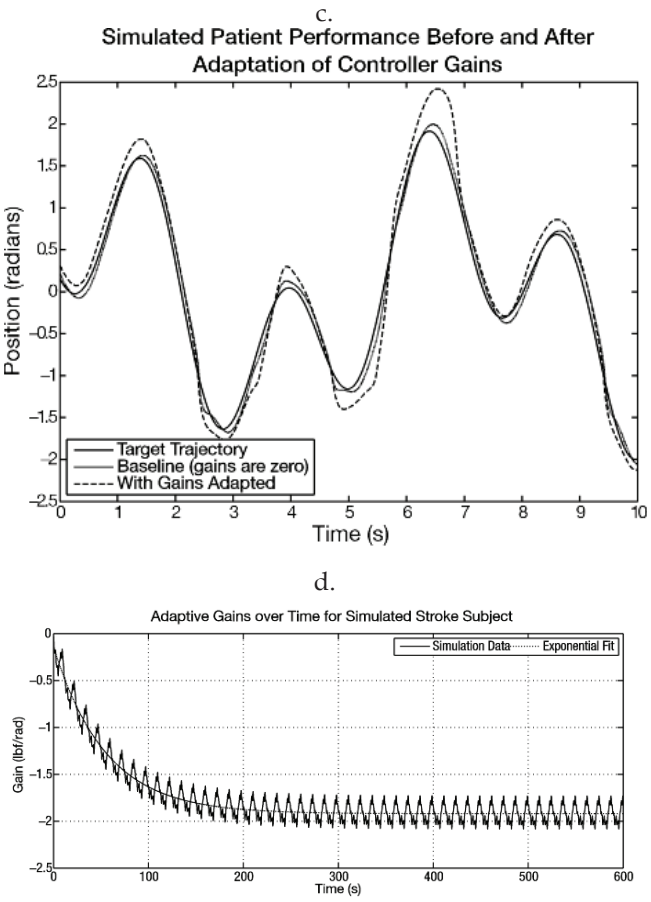

Fig. 8c. Simulated Healthy patient's performance before and after gains are being adapted. 8d. Rendered stiffness adapting to simulated stroke patient over time. More negative values indicate more assistive gains

4.2 Case Studies

Stroke subject is shown tracking a trajectory with zero-impedance and the position dependent adaptive mode in Figure 10. The stroke subject was less able to track the sinusoid than the healthy subject. This was reflected in their level of accuracy where RMS error for stroke survivor was greater (0.62 versus 0.2040). The position adaptive controller was representative of our adaptive mode; the controller further reduced the RMS error to 0.346. This indicates that the subject was given the assistance needed to enable tracking (Figure 10b). The adaptive controller slightly increased the tracking error of the healthy subject from 0.2040 to 0.287. This is because the controller will work to provide more resistance to increase tracking challenge if the subject tracking error was less than 0.2. Fig. 10c depicts the baseline RMS tracking error of a stroke subject during exercises in zero-impedance mode. Superimposed on this data is the position-dependent adaptive

controller gain after it had reached steady state. Compared to the simulation data shown in Fig. 9, the real data in Fig. 10c displays the same trend. At the points at which the subject has the greatest tracking error, the adaptive controller provides a greater amount of assistance. This is shown by the two peaks in the plot of RMS tracking error, which is reflected in the shape of the plot of adaptive controller gain. The peaks in adaptive gain are wider due to the use of a spatial smoothing window in the adaptive algorithm (this smoothing caused the two peaks to merge

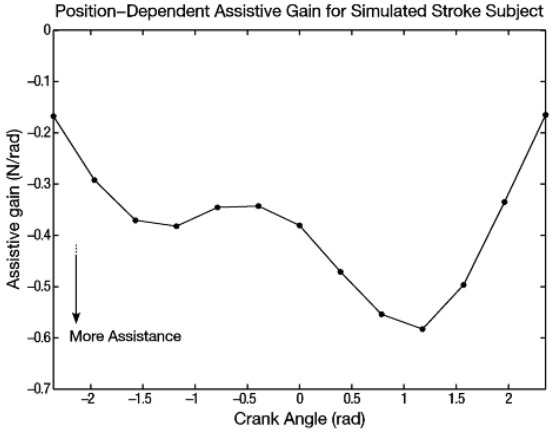

Fig. 9. Position dependent gains adapting to simulated stroke patient's performance.

together partially).

5 Discussion

5.1 Design

The hardware developed for the haptic robot satisfies the first goal of being a drop-in replacement for the Logitech wheel by mounting to the same frame and interfacing physically with human subjects in the same manner. The second specific aim is fulfilled by the robot's high force output, which enables the robot to provide assistance to subjects who are too weak or too uncoordinated to use the Logitech wheel. By emulating the main features of the UniTherapy software, the haptic robot's software presents subjects with an interface that has the same look and feel of UniTherapy, fulfilling the first specific aim. The adaptive control software provides more flexibility than UniTherapy in the way assistance/resistance is applied to the human subject, which allows therapy to be personalized to each subject; this fulfills the second specific aim of extending accommodations to low-functioning subjects.

The biggest shortcoming of the haptic robot is the performance of its motor. The treadmill motor is designed to spin in one direction at a constant speed, not to provide smooth motion at near-stall speeds. Because of this, the motor has a low number of windings on the armature, which leads to noticeable cogging effects at slow speeds. The low number of windings also causes the torque constant of the motor to be position-dependent, leading to inconsistent performance of the impedance controller. A motor designed specifically as a servo would offer superior performance, but budget and weight constraints did not permit such a motor to be used. Because the robot lacks a "dead-man" switch on the crank handle, it has no means to sense whether a user is in contact with the end-effector. The handle grip spins freely, so a switch cannot be installed in it without risk of damage to the wiring. This creates a safety concern because the impedance controller is unstable if there is nothing in contact with the end effector. Due to this concern, subjects wear a grasp-assist glove that prevents them from releasing the handle, and perform exercises under close supervision. These safety measures are not an ideal solution as the glove does not fit all people. It is recommended that the handle be modified to accept a "dead-man" switch or similar device in order to enhance the current safety measures.

5.2 Evaluation

The adaptive controller simulation experiments were successful in that the data recorded supports both hypotheses. The plots of gain over time in Figures 8b and 8d both show a general first-order trend, neglecting the oscillations, and Figure 9 shows the position-dependent adaptive controller assigning the highest gains to regions with the highest tracking errors. The controller also shows sensitivity to impairment level, as seen by the difference in steady-state gain between the healthy arm in Figure 8a and the stroke-impaired arm is Figure 8c.

The first-order trend of controller gain is similar to the results seen in the Wrist-Robot experiment and other robot controllers [18]. Subjects tracked oscillating trajectories using the robot, and the adaptive controller increased the oscillation frequency proportional to the subject's performance. Because of this relationship between performance and frequency, oscillation frequency for the Wrist-Robot is an analog to rendered spring stiffness in the haptic TheraDrive robot, as both these parameters modulate exercise difficulty. Wrist oscillation frequency with the Wrist-Robot showed the same first-order response characteristic in each of the eleven exercises.

A weakness in the simulation's adaptive controller is that the assistive/resisitive gain oscillates at steady state. These oscillations are stable, as they do not grow exponentially as the exercises progress, and they are a phenomenon caused by the shape of the exercise trajectory, as the two have the same period (12.6 seconds in Figure 8d). A similar phenomenon was mentioned by Vergaro et al. as a frequent occurrence in continuously-adapted controllers [18]. Methods of removing these oscillations include increasing the length of the window used to calculate RMS tracking error and decreasing the adaptation gain. However, both these methods slow the rate of adaptation and make the controller less responsive to sudden spikes in tracking error that occur when, for example, a stroke subject becomes stuck in one position. Ultimately, the oscillations are inseparably linked to the trajectory, and eliminating them would cause an unacceptable loss of controller performance.

However, the oscillation is small enough that it is imperceptible to patients, as the exercises themselves pre-

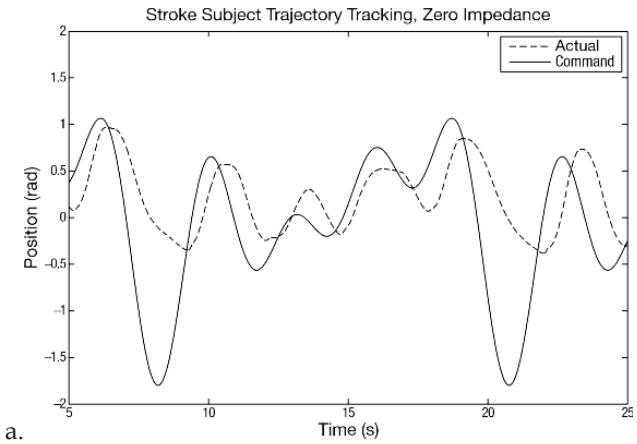

a.

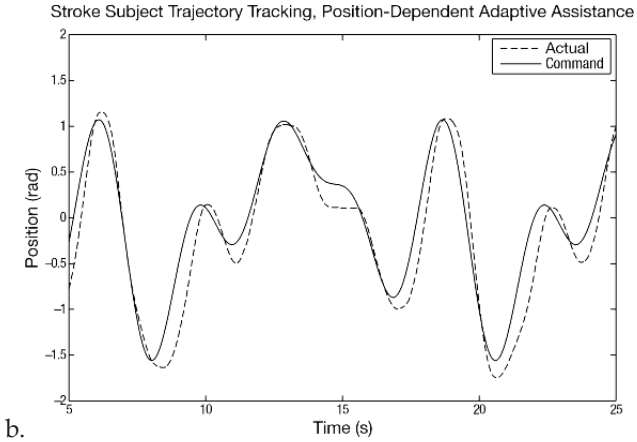

b.

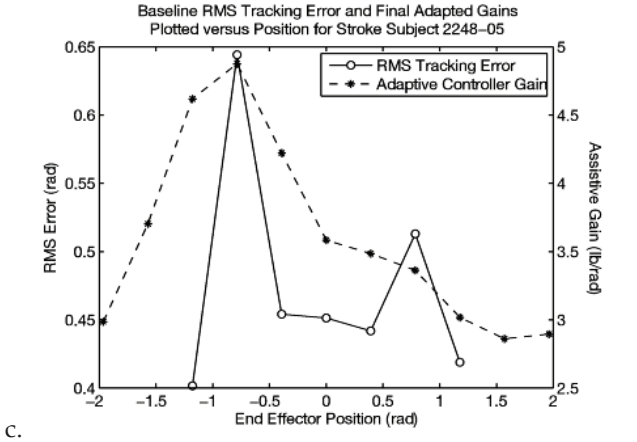

c.

Fig. 10abc. Stroke subject completing twomodes: a) zero-impedance mode , b) an adaptive mode and c) s the position-dependent gains changing and adapting over time.

sent variations of force of much greater magnitude and speed than those caused by small variations of stiffness.

Position-dependent gains developed as hypothesized.

The largest assistive gains were seen in the positions where the simulated subject's tracking error was at a maximum, which in turn correspond loosely to the points where the trajectory perturbation to simulate stroke was largest. Figures 9 and 10c shows that the position-dependent adaptive controller fits the ``assist as needed'' paradigm; it is able to provide extra assistance only where it is necessary to maintain subject performance.

Although it was modified to work in the haptic robot simulations, the MIT-Manus arm model still behaved as it did in simulations discussed by Formica et al [20]. The tracking error of the arm model showed sensitivity both to the level of assistance provided and to the level of impairment modeled.

The simulated stroke subject model in Figure 8a behaves nothing like the real stroke subject in Figure 10ab when tracking trajectories in zero-impedance mode. The real stroke shows a limited range of motion and a noticeable delay of movement. Spatially, the trajectory the real stroke subject follows is very similar to the commanded trajectory when inside the subject's limited range of motion; none of the perturbations present in the simulated stroke model appear in the real subject. These differences stem from the fact that the MIT-Manus arm model was intended to simulate stroke subjects performing point-to-point movements on a tabletop. The Manus simulation model imitated the zig-zag paths that real stroke subjects took during movements between points [21]. Using this model with a crank constraint and a pre-defined trajectory did not produce behavior seen in real stroke subjects because the model was not being used for its intended purpose. The simulation had utility in validation and proof of method. There is a need to improve the model.

6 Conclusion

A haptic therapy robot, Haptic Theradrive, was designed to accommodate stroke survivors with a wide range of functional ability and assist them safely. A novel compliant torque limiter was implemented to allow the system to be used safely despite its large torque capacity. The torque limiter would be preset for the patient before the system could be used independently. An adaptive controller adds the ability to keep the tracking tasks challenging yet doable. Low functioning stroke survivors are now able to benefit from the system.

Human subject pilot studies are being conducted to assess the utility of the various control schemes in providing a challenging and engaging therapy environment. From these studies, the Haptic TheraDrive will be compared to the original system.

Acknowledgment

This work was supported in part by the American Heart Association under grant #0635450Z entitled “Robot-Assisted Motivating Rehabilitation after Stroke” and by department funds of the Physical Medicine and Rehabilitation of the Medical College of Wisconsin. We also extend our thanks to members of the Rehabilitation Robotics Research and Design Lab. Direct all correspondence to Dr. Michelle J. Johnson.

References

[1] N. F. Gordon, M. Gulanick, F. Costa, G. Fletcher, B. A. Franklin, E. J. Roth, and T. Shephard, “Physical activity and exercise rec-

ommendations for stroke survivors: An american heart association scientific statement from the council on clinical cardiology, subcommittee on exercise, cardiac rehabilitation, and prevention; the council on cardiovascular nursing; the council on nutrition, physical activity, and metabolism; and the stroke council," Stroke, vol. 35, pp. 1230–1240, May 2004.

[2] C. V. Loureiro, W. S. Harwin, K. Nagai, M.J. Johnson, "Advances in upper limb stroke rehabilitation: a technology push, Med Biol Eng Comput." vol. 49, no. 10, pp. 1103-1118, 2011.

[3] A.C. Lo, P. Guarino, L.G. Richards, J.K. Haselkorn, G.F. Wittenberg, D.G. Federman, R. J. Ringer, T.H. Wagner, H.I. Krebs, B.T. Volpe, C. T. Bever Jr, D.M. Bravata, P.W. Duncan, B.H. Corn, A.D. Maffucci, S.E. Nadeau, S.S. Conroy, J.M. Powell, G.D. Huang, P. Peduzzi, "Robot-assisted therapy for long-term upper-limb impairment after stroke." N Engl J Med. Vol. 362, pp. 1772-83. 2010

[4] S. R. Wood, N. Murillo, P. B. y Rita, R. S. Leder, J. T. Marks, and S. J. Page, "Motivating, game-based stroke rehabilitation: A brief report," Topics in Stroke Rehabilitation, vol. 10, no. 2, pp. 134–140, October 2003.

[5] M. J. Johnson, H. F. M. Van der Loos, C. G. Burgar, P. Shor, and L. J. Leifer, "Experimental results using force-feedback cueing in robotassisted stroke therapy," IEEE Transactions on Neural Systems and Rehabilitation Engineering, vol. 13, no. 3, pp. 335–348, September 2005.

[6] D. J. Reinkensmeyer, C. T. Pang, J. A. Nessler, and C. C. Painter, "Web-based telerehabilitation for the upper extremity after stroke," IEEE Transactions on Neural Systems and Rehabilitation Engineering, vol. 10, no. 2, pp. 102–108, 2002.

[7] M. J. Johnson, X. Feng, L. M. Johnson, and J. M. Winters, "Potential of a suite of robot/computer-assisted motivating systems for personalized, home-based, stroke rehabilitation," Journal of NeuroEngineering and Rehabilitation, vol. 3, p. 29, March 2007.

[8] X. Feng and J. M. Winters, "A pilot study evaluating use of a computer-assisted neurorehabilitation platform for upperextremity stroke assessment," Journal of NeuroEngineering and Rehabilitation, May 2009.

[9] R. Ruparel, M. J. Johnson, E. Strachota, J. McGuire, and G. Tchekanov, "Evaluation of the theradrive system for robot/computer assisted motivating rehabilitation after stroke," in 31st Annual International IEEE EMBS Conference, April 2009, pp. 811–814.

[10] M.J Johnson, M. Trickey, E. Brauer, F. Xin, "TheraDrive: A new stroke therapy concept for home-based computer-assisted motivating rehabilitation,"in Conf Proc IEEE Eng Med Biol Soc 2: September 2004.pp. 4844-47,

[11] R. Colombo, F. Pisano, A. Mazzone, C. Delconte, S. Micera, M.C. Carrozza, P. Dario, and G. Minuco, "Design Strategies to Improve Patient Motivation during Robot-Aided NeuroRehabilitation." J NeuroEngineering and Rehabil, vol. 4, no. 6, Mar 1 2007.

[12] S. Hesse, C. Werner, M. Pohl, S. Rueckriem, J. Mehrholz, and M.L. Lingnau. "Computerized arm training improves the motor control of the severely affected arm after stroke: A single-blinded randomized trial in two centers." Stroke. vol. 36, pp. 1960-1966, 2005

[13] L. Masia, M. Casadio, P. Giannoni, G. Sandini, and P. Morasso,"Performance adaptive training control strategy for recovering wrist movements in stroke patients: a preliminary, feasibility study," Journal of Neuroengineering and Rehabilitation, vol. 6, no. 1, p. 44, December 2009.

[14] R. van Ham, T. G. Sugar, B. Vanderborght, K. W. Hollander, and D. Lefeber, "Compliant actuator designs: Review of actuators with passive adjustable compliance/controllable stiffness for robotic applications," IEEE Robotics & Automation Magazine, vol. 16, no. 3, pp. 81–94, September 2009.

[15] S. Wolf and G. Hirzinger, "A new variable stiffness design: Matching requirements of the next robot generation," in IEEE International Conference on Robotics and Automation, May 2008, pp. 1741–1746.

[16] J. L. Emken, R. Benitez, and D. J. Reinkensmeyer, "Humanrobot cooperative movement training: Learning a novel sensory motor transformation during walking with robotic assistance-asneeded," Journal of Neuroengineering and Rehabilitation, vol. 4, March 2007, pp. 8.

[17] R. Riener, L. Lunenburger, S. Jezernik, M. Anderschitz, G. Colombo, and V. Dietz, "Patient-cooperative strategies for robot-aided treadmill training: first experimental results," IEEE Trans Neural Syst Rehabil Eng, vol 13, pp. 380-394, 2005.

[18] R. Colombo, I. Sterpi, A. Mazzone, C. Delconte, and F. Pisano. Taking a lesson from patients' recovery strategies to optimize training during robot-aided rehabilitation. IEEE Trans Neural Syst Rehabil Eng vol 20, pp. 276-285, 2012.

[19] E. Vergaro, M. Casadio, V. Squeri, P. Giannoni, P. Morasso, and V. Sanguineti., "Self-adaptive robot training of stroke survivors for continuous tracking movements," J Neuroeng Rehabil vol. 7, no. 13, 2012

[20] M. Casadio, P. Giannoni, L. Masia, P. Morasso, G. Sandini, V. Sanguineti,V. Squeri, E. Vergaro. "Robot therapy of the upper limb in stroke patients: preliminary experiences for the principle-based use of this technology," Func Neuro vol. 24, no. 195. 2009

[21] A. R. Theriault, M. L. Nagurka, and M. J. Johnson, "A robust wheel interface with a novel adaptive controller for computer/robot-assisted motivating rehabilitation," in ASME International Symposium on Flexible Automation, June 2012.

[22] D. Formica, L. Zollo, and E. Guglielmelli, "Torque-dependent compliance control in the joint space of an operational robotic machine for motor therapy," in IEEE 9th International Conference on Rehabilitation Robotics, June 2005, pp. 341–344.

[23] A. R. Fugl-Meyer, L. Jääskö, I. Leyman, S. Olsson, and S. Steglind, "The post-stroke hemiplegic patient: A method for evaluation of physical performance," Scandinavian journal of rehabilitation medicine, vol. 7, no. 1, pp. 13, 1975.

Andrew Theriault, M.S., received the Honors B.S. in Biomedical Engineering and M.S. in Mechanical Engineering from Marquette University, where he was co-advised by Drs. Johnson and Nagurka. He is currently a research assistant to Dr. Johnson, working with upper-extremity rehabilitation robots. His research interests include robotics, haptics, and machine design. He is a student member of ASME.

Mark Nagurka, PhD., received his B.S. and M.S. in Mechanical Engineering and Applied Mechanics from the University of Pennsylvania in 1978 and 1979, respectively, and a Ph.D. in Mechanical Engineeringfrom M.I.T. in 1983. Prior to joining Marquette University, he taught at Carnegie Mellon University and was a Senior Research Engineer at the Carnegie Mellon Research Institute. Dr. Nagurka is a registered Professional Engineer in Wisconsin and Pennsylvania, a Fellow of the American Society of Mechanical Engineers (ASME), and a former Fulbright Scholar. His research interests include design of mechanical and electromechanical systems, design of control systems, mechatronics, automation, human/machine interaction, and vehicle dynamics.

Michelle J. Johnson, PhD., received her B.S. in Mechanical Engineering and Applied Mechanics from the University of Pennsylvania and her M.S. in Mechanical Engineering from the University of California, Irvine. Her PhD is in Mechanical Engineering, with an emphasis in mechatronics, robotics, and design, from Stanford University. She completed a NSF-NATO post-doctoral fellowship at the Advanced Robotics Technology and Systems Laboratory at the Scuola Superiore Sant'Anna in Italy. Dr. Johnson is now an Assistant Professor at the University of Pennsylvania.